Efficient Modeling of Spin Evolutions In Precessing Neutron Star Binaries

Quinn Kasdan-Grollo, Giulia Fumagalli, and Taylor Knapp
(Dated: September 25, 2026)

Spin-induced precession in a compact binary has a significant impact on both the detected gravitational wave signal and the binary's evolution history, making modeling precessing compact binaries an interesting avenue for study. We extend upon the post-Newtonian framework developed by Gerosa *et al.*, which modeled the evolution of precessing black hole binaries, to the unexplored regime of binary neutron stars (BNSs). We generalize the spin-precession equations to quasi-circular BNS systems, where determining the allowed precession ranges of the angular momentum vectors is less analytically tractable than in the binary black hole (BBH) case. To resolve this, we identify restrictive physical bounds on the interpolation grid used to find the aforementioned precession bounds, further optimize the interpolation grid, and compactify spin-precession equations making evolution of precessing BNSs robust and efficient. This new framework for modeling BNSs efficiently tracks the evolution of spin directions throughout the entire inspiral, enabling study of the impact of matter effects on spin precession. Understanding this impact has the potential for constraining neutron star equations of state through study of real event spin evolutions, which will be especially relevant for next-generation gravitational wave detectors that can observe the long BNS inspiral.

I. INTRODUCTION

The LIGO/Virgo/KAGRA (LVK) collaboration's observational focus falls on stellar mass compact binaries – binaries with black holes (BHs) and neutron stars (NSs). In these relativistic systems, the spin of the objects interacts with themselves and the orbital angular momentum of the binary, which can lead to precession of the orbital plane [2–4]. This wobbling of the orbital plane impacts the signal LVK detectors observe. Moreover, we can gain information about the compact binary with proper characterization of precession from detected signals. Thus, modeling the precessional behavior of compact binary systems is important for compact binary studies and LVK detections.

Precession can be modeled by numerically solving Einstein's equations via numerical relativity (NR) or by using a post-Newtonian (PN) approach where relativistic corrections to Newtonian dynamics are added to match general relativity. Using NR is the most accurate choice, but to use NR to study precession across a large population of compact binaries would be prohibitive due to how computationally expensive it is. Meanwhile, the PN approach allows for the inclusion of relativistic effects that drive precession without requiring supercomputers and months of time. We thus seek a way to model precessing systems with PN in hopes of accurate and computationally efficient precession models.

Gerosa *et al.* found a way to make calculations even faster by utilizing a helpful timescale hierarchy. This allowed for 'precession averaging', i.e. averaging out the spin behavior over a precessional period, of precessing BBHs. This process makes evolving BBHs from large separations to close to merger ($r > 10\frac{GM}{c^2}$) incredibly efficient, and has been used to better understand different spin configurations and formation channels of BBHs.

However, extending this framework to precessing BNSs is complex. In the BBH case, the equation whose roots determine the bounds for precession averaging is a cubic polynomial, this makes finding the bounds for precession averaging analytical. In generalizing to BNSs, we are left with a non-polynomial expression and cannot find closed form solutions for the bounds of precession.

In this paper, we extend upon the framework developed by Gerosa *et al.* by generalizing the precession dynamics to BNSs. We find a more complex equation that dictates BNS precession and makes extending to precession averaging non-trivial. We then simplify this new form to a six-degree polynomial, and thus are able to model precessing BNSs with similar CPU times to the BBH case. We also find spin configurations unique to BNSs. Our results allow for investigation of BNS spin configurations and their relation to BNS formation channels, as well as the impact of the NS equations of state (EOSs) on spin configurations.

Note that from here on out we will use geometrical units where $G = c = 1$.

II. BACKGROUND

A. Spin-Induced Precession

In spinning compact binaries there are three main effects that influence precession. At 1.5PN, spin-orbit coupling occurs as a result of spinning compact objects dragging the space-time around them, this affects the orbit and spin orientations of the system [2]. At 2PN, spin-spin couplings and the spin-induced quadropole-monopole moment interaction further influences the compact binary dynamics [3, 4]. In interacting with the orbit and spin, these effects can lead to precession. Precession will occur when the total spin vector $\mathbf{S} = \mathbf{S}_1 + \mathbf{S}_2$ is misaligned with the orbital angular momentum $\mathbf{L}$, where $\mathbf{S}_1$ and $\mathbf{S}_2$ are the spins of compact objects 1 and 2,

respectively. Precession occurs about the system's total angular momentum vector, $\mathbf{J} = \mathbf{S} + \mathbf{L}$. A useful graphic showing this set up and the precession of $\mathbf{L}$ about $\mathbf{J}$ can be found in Figure 1.

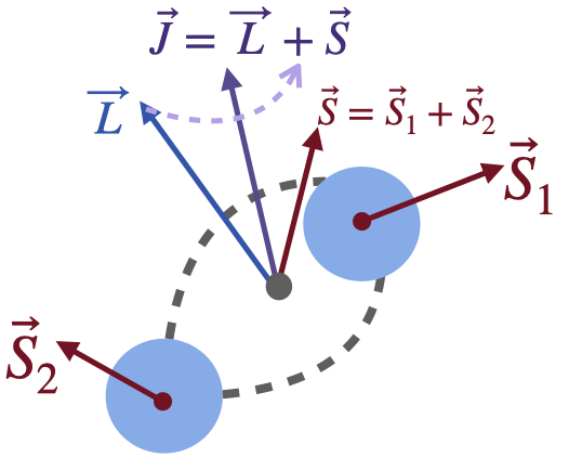


FIG. 1. This graphic gives a clear look at the different angular momentum vectors in a spinning binary system – $\mathbf{S}_1$, $\mathbf{S}_2$, $\mathbf{L}$, and $\mathbf{J}$.

B. The Timescale Hierarchy

At 2PN, the treatment of precessing compact binaries admits a timescale hierarchy which greatly simplifies the problem: the orbital motion takes place on $t_{\rm orb} \propto (r/M)^{3/2}$ while the spins precess on $t_{\rm pre} \propto (r/M)^{5/2}$ [1]. That is, for sufficiently large separations, $t_{\rm orb} \ll t_{\rm pre}$, i.e. multiple orbits occur before precession of the spins and orbital plane changes their orientation significantly. Ref. [2] uses this hierarchy to employ the method of "orbit averaging" to describe the change in spin and orbital angular momentum throughout inspiral. This allows for the study of the effects of precession over a few precession cycles.

However, when studying compact binary dynamics from formation to merger, orbit averaging is too computationally expensive. Modeling over an entire inspiral requires tracking the orientations of spin and momentum vectors at each time step during integration. Storing all this information makes orbit averaging quite slow. Gerosa *et al.* find a way to overcome this limitation by utilizing the full timescale hierarchy for $r > 10M$. Since $t_{\rm RR} \propto (r/M)^4$,

$$t_{\rm orb} \ll t_{\rm pre} \ll t_{\rm RR}. \tag{1}$$

Just as orbit averaging relies on $t_{\rm orb} \ll t_{\rm pre}$, the right hand side of the hierarchy, $t_{\rm pre} \ll t_{\rm RR}$, opens up the opportunity for precession averaging. Precession averaging is helpful as it takes away the need to track the exact precessional phase. Instead of storing the orientations of angular momentum vectors at each time step, we can simply track a scalar evolution of spin direction throughout inspiral. This allows for the recovery of all relevant information about the BNS much more efficiently. Ref. [5] does this by rewriting the 2PN orbit-averaged spin equations, as described in Section II D. In doing so, Ref. [5] developed a way to understand the evolution of the "shape" of precession throughout inspiral efficiently.

C. Physical Setup in a Co-Precessing Frame

Following the set up in Ref. [1], we consider a compact binary with masses $m_1 \geq m_2$. The total mass $M = m_1 + m_2$ does not affect the shape of the problem, only the scale, thus we set it to $M = 1$ in our numerical implementation. The mass ratio is defined as $q = m_2/m_1 \in (0, 1]$ and the Kerr spin parameters as $\chi_{1,2} = S_i/m_i^2 \in [0, 1)$. The spin magnitudes are given as:

$$S_1 = \frac{\chi_1}{(1+q)^2} M^2\,, \tag{2}$$

$$S_2 = \frac{q^2 \chi_2}{(1+q)^2} M^2\,. \tag{3}$$

In this project we restrict our focus to quasi-circular orbits, leaving the orbital angular momentum to be expressed as

$$L = M^2 \frac{q}{(1+q)^2} \sqrt{\frac{r}{M}}\,, \tag{4}$$

and the compactified coordinate, introduced in, Ref. [5] as

$$u = \frac{1}{2L}\,, \tag{5}$$

where $u \to 0$ as $r \to \infty$.

In a co-precessing frame, we fix the z-axis to $\mathbf{L}$ and we describe the orientations of our spin and momentum vectors with three angles, the angles between the spins and orbital angular momentum, $\theta_{1,2} \in [0, \pi]$ and the azimuthal angle $\Delta\Phi \in [-\pi, \pi]$ between the projections of the spins onto the xy-plane. These are defined by,

$$\cos\theta_1 = \hat{\mathbf{S}}_\mathbf{1} \cdot \hat{\mathbf{L}}, \tag{6}$$

$$\cos\theta_2 = \hat{\mathbf{S}}_\mathbf{2} \cdot \hat{\mathbf{L}}, \tag{7}$$

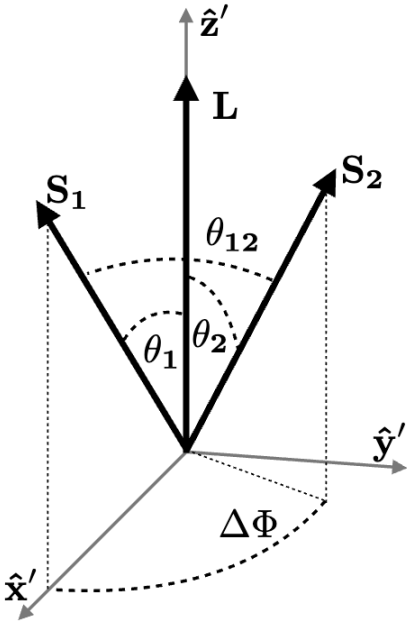


FIG. 2. The co-precessing frame used by Ref. [5] that our work handles. Included in the figure are the spins $\mathbf{S}_{1,2}$ and orbital angular momentum $\mathbf{L}$, and angles described in Equations (6) - (8).

and

$$\cos\Delta\Phi = \frac{\hat{\mathbf{S}}_1 \times \hat{\mathbf{L}}}{|\hat{\mathbf{S}}_1 \times \hat{\mathbf{L}}|} \cdot \frac{\hat{\mathbf{S}}_2 \times \hat{\mathbf{L}}}{|\hat{\mathbf{S}}_2 \times \hat{\mathbf{L}}|}, \tag{8}$$

$$\mathrm{sgn}\Delta\Phi = \mathrm{sgn}\{\mathbf{L} \cdot [(\mathbf{S}_1 \times \mathbf{L}) \times (\mathbf{S}_2 \times \mathbf{L})]\}. \tag{9}$$

With these definitions we fully capture the orientations and magnitudes of our quantities of interest. Figure 2 shows these vectors and angles clearly.

D. Constants of motion & spin evolution dynamics

To understand the usefulness of precession averaging, we first present the 9-dimensional problem described by the 2PN orbit-averaged equations of motion. Then we will see how the problem is simplified with the methods used in Ref [1].

Klein provides the 9-dimensional problem we are left to solve with the 2PN orbit-averaged approach:

$$\frac{d\boldsymbol{S}_1}{dt} = \frac{1}{2r^3}[\mathcal{S}_1\boldsymbol{L} + \boldsymbol{S}_2] \times \boldsymbol{S}_1\,, \tag{10}$$

$$\frac{d\boldsymbol{S}_2}{dt} = \frac{1}{2r^3}[\mathcal{S}_2\boldsymbol{L} + \boldsymbol{S}_1] \times \boldsymbol{S}_2\,, \tag{11}$$

and

$$\frac{d\boldsymbol{L}}{dt} = \frac{1}{2r^3}[\mathcal{S}_1\boldsymbol{S}_1 + \mathcal{S}_2\boldsymbol{S}_2] \times \boldsymbol{L} + \frac{dL}{dt}\hat{\boldsymbol{L}}\,, \tag{12}$$

where,

$$\mathcal{S}_1 = 4 + 3q - \frac{3(1+q)^2}{\sqrt{r/M}}(k_1\boldsymbol{S}_1 + \frac{\boldsymbol{S}_2}{q}) \cdot \frac{\hat{\boldsymbol{L}}}{M^2} \tag{13}$$

and

$$\mathcal{S}_2 = 4 + \frac{3}{q} - \frac{3(1+q)^2}{q\sqrt{r/M}}(\boldsymbol{S}_1 + k_2\frac{\boldsymbol{S}_2}{q}) \cdot \frac{\hat{\boldsymbol{L}}}{M^2}\,. \tag{14}$$

In equations (13) and (14) the k_1 and k_2 terms are a scalar quantity related to the tidal deformability of objects 1 and 2 – for BBHs $k_1 = k_2 = 1$. In Equation (12), the $\frac{dL}{dt}$ term captures the loss of energy due to radiation reaction. Though, as discussed in Section II B, this has a negligible effect over one precessional cycle and can be set to 0 on $t_{\rm pre}$ for our purposes.

To capture the spin dynamics and evolution in a compact way, one can use the spin quantity commonly measured by LVK observations – $\chi_{\rm eff}$,

$$\begin{aligned}\chi_{\rm eff} &\equiv \frac{(1+q)}{M^2}\left(\mathbf{S}_1 \cdot \hat{\mathbf{L}} + \frac{\mathbf{S}_2 \cdot \hat{\mathbf{L}}}{q}\right) \\ &= \frac{\chi_1\cos\theta_1 + q\chi_2\cos\theta_2}{1+q}\,,\end{aligned} \tag{15}$$

paired with the "weighted spin-difference" $\delta\chi$,

$$\begin{aligned}\delta\chi &\equiv \frac{(1+q)}{M^2}\left(\mathbf{S}_1 \cdot \hat{\mathbf{L}} - \frac{\mathbf{S}_2 \cdot \hat{\mathbf{L}}}{q}\right) \\ &= \frac{\chi_1\cos\theta_1 - q\chi_2\cos\theta_2}{1+q}\,,\end{aligned} \tag{16}$$

formulated by Ref. [4] and Ref. [6] respectively. $\chi_{\rm eff}$ is conserved on $t_{\rm pre}$ and $t_{\rm RR}$.

Also conserved on $t_{\rm pre}$ is J and L, so we introduce the "asymptotic angular momentum",

$$\kappa = \frac{J^2 - L^2}{2L}\,, \tag{17}$$

which must be conserved on $t_{\rm pre}$ since J and L are.

Combined, $\delta\chi$, $\chi_{\rm eff}$, and κ carry all relevant information about a compact binary, with only $\delta\chi$ varying on $t_{\rm pre}$. Thus, we only need its time derivative $\dot{\delta\chi}$ to describe the change direction of in angular momentum vectors on the precessional timescale (we occasionally use dot notation to signify a time derivative). As described in Section II E, the two values that $\delta\chi$ oscillates between on $t_{\rm pre}$ are what we can use to precession average.

With our re-parameterization, Equations (10) - (12), and Equations (17) - (20) in Ref. [1], we can express the orbit-averaged evolution of $\chi_{\rm eff}$ and $\delta\chi$ as,

$$M\frac{d\chi_{\rm eff}}{dt} = \frac{3}{4}\left(\frac{M}{r}\right)^{7/2}\frac{q\chi_1\chi_2}{(1+q)^2}[\chi_{\rm eff}(k_1-k_2)+\delta\chi(k_1+k_2-2)]\hat{\mathbf{L}}\cdot(\hat{\mathbf{S}}_{\mathbf{1}}\times\hat{\mathbf{S}}_{\mathbf{2}})\,, \tag{18}$$

$$M\frac{d\delta\chi}{dt} = -\frac{3}{4}\frac{M^3}{r^{7/2}}\frac{q\chi_1\chi_2}{(1+q)^2}\{-4\sqrt{r}+\sqrt{M}[\chi_{\rm eff}(2+k_1+k_2)+\delta\chi(k_1-k_2)]\}\mathbf{L}\cdot(\hat{\mathbf{S}}_{\mathbf{1}}\times\hat{\mathbf{S}}_{\mathbf{2}})\,. \tag{19}$$

In the BBH case, since $k_1 = k_2 = 1$, Equation (18) goes to 0, leaving Equation (19) to fully describe the spin dynamics up to $r > 10M$.

In the BNS case $\chi_{\rm eff}$ is no longer constant on $t_{\rm pre}$. Instead Fumagalli *et al.* finds,

$$\chi_{\rm cons} = \frac{2\left(\chi_{\rm eff}^2+\chi_{\rm quad}^2\right)}{1+\sqrt{1-\frac{2}{\sqrt{r/M}}\left(\chi_{\rm eff}-\frac{\chi_{\rm eff}^2+\chi_{\rm quad}^2}{2\sqrt{r/M}}\right)}}\,, \tag{20}$$

where

$$\chi_{\rm quad}^2 \equiv \frac{1}{M^2}\left[(k_1-1)\left(\frac{\boldsymbol{S}_1\cdot\hat{\boldsymbol{L}}}{m_1}\right)^2+(k_2-1)\left(\frac{\boldsymbol{S}_2\cdot\hat{\boldsymbol{L}}}{m_2}\right)^2\right] \tag{21}$$
$$= \frac{(k_1-1)(\chi_1\cos\theta_1)^2+(k_2-1)(q\chi_2\cos\theta_2)^2}{(1+q)^2}\,.$$

$\chi_{\rm cons}$ is constant on $t_{\rm pre}$ and reduces to $\chi_{\rm eff}$ in both the BH limit $k_1 = k_2 = 1$ and the Newtonian limit $r \to \infty$.

With this generalization to $\chi_{\rm eff}$, we can again describe our binary with two quantities $\delta\chi$ and $\chi_{\rm cons}$. Since $\chi_{\rm cons}$ is constant on $t_{\rm pre}$ we only need to track the evolution of $\delta\chi$ with Equation (19), just as in the BBH case.

In summary, compact binaries in quasi-circular orbits can be parameterized using $q, \chi_1, \chi_2, \chi_{\rm cons}, u, \kappa$, and $\delta\chi$. On $t_{\rm pre}$, since the effects of radiation reaction do not decrease (increase) the orbital separation r (compactified coordinate u) significantly, u and κ are constant. Also constant on $t_{\rm pre}$ is $\chi_{\rm cons}$. Constant throughout inspiral are q, χ_1, and χ_2.

E. Precession Averaging

To average a generic quantity X over a precessional cycle characterized by the precessional period,

$$\tau_{\rm pre} = 2\int_{\delta\chi_-}^{\delta\chi_+}\left(\frac{d\delta\chi}{dt}\right)^{-1}d\delta\chi\,, \tag{22}$$

we perform the following calculation,

$$\langle X\rangle = \frac{\int_{\delta\chi_-}^{\delta\chi_+} X(\delta\chi)\left(\frac{d\delta\chi}{dt}\right)^{-1}d\delta\chi}{\tau_{\rm pre}}\,, \tag{23}$$

$$\left(\frac{d\delta\chi}{dt}\right)^2 = \mathcal{A}^2(1-\cos^2\theta_1)(1-\cos^2\theta_2)(1-\cos^2\Delta\Phi)\,, \tag{24}$$

where $\delta\chi_-$ and $\delta\chi_+$ are the roots of the right-hand side of Equation (19). For the generalized compact binary case, Equation (19) takes the form:

where,

$$\mathcal{A} = \frac{3M^3 q\chi_1\chi_2\sqrt{\delta\chi^2 M(1-k_1k_2) - 2\sqrt{M}\sqrt{r}\left[\delta\chi(k_1-k_2)+\chi_{\rm cons}(k_1+k_2+2)\right] + M\chi^2_{\rm cons}(k_1+k_2+2)+4r}}{2(1+q)^2 r^{7/2}}\,, \tag{25}$$

$$\cos\theta_1 = \frac{(1+q)\left[2\sqrt{r/M}+(1+k_2)\delta\chi\right]}{(2+k_1+k_2)\chi_1}$$

$$-\frac{(1+q)\sqrt{4r/M+(1-k_1k_2)\delta\chi^2+(2+k_1+k_2)\chi^2_{\rm cons}-2\sqrt{r}\left[(k_1-k_2)\delta\chi+(2+k_1+k_2)\chi_{\rm cons}\right]}}{(2+k_1+k_2)\chi_1}, \tag{26}$$

$$\cos\theta_2 = \frac{(1+q)\left[2\sqrt{r/M}-(1+k_1)\delta\chi\right]}{q(2+k_1+k_2)\chi_2}$$

$$-\frac{(1+q)\sqrt{4r/M+(1-k_1k_2)\delta\chi^2+(2+k_1+k_2)\chi^2_{\rm cons}-2\sqrt{r}\left[(k_1-k_2)\delta\chi+(2+k_1+k_2)\chi_{\rm cons}\right]}}{q(2+k_1+k_2)\chi_2}\,, \tag{27}$$

and

$$\cos\Delta\Phi = \frac{2kq(q+1)^2\sqrt{r} - M^2\left[2q\chi_1\cos\theta_1\left(q\chi_2\sqrt{M}\cos\theta_2+\sqrt{r}\right)+2q^3\chi_2\sqrt{r}\cos\theta_2+\sqrt{M}\left(q^4\chi_2^2+\chi_1^2\right)\right]}{2M^{5/2}q^2\chi_1\chi_2\sin\theta_1\sin\theta_2}\,. \tag{28}$$

While $\mathcal{A}^2$, $\sin^2\theta_1$, and $\sin^2\theta_2$ have closed form solutions, $\sin^2\Delta\Phi$ does not. This makes finding the roots of Equation (24) nontrivial, interpolating the function across a grid of $\delta\chi$ values to obtain the roots is possible, but not robust. That being said, we do have a way to precession average a BNS inspiral with this generalization.

Finally, we must track the important quantities that evolve on t_{RR}: u, κ, and $\chi_{\rm cons}$. We can express the evolutions of κ and $\chi_{\rm cons}$ as functions of u and precession average their expressions,

$$\frac{d\kappa}{du} = \langle S^2\rangle\,, \tag{29}$$

where

$$S^2 = \frac{M^2}{u}\left[\frac{\kappa}{M^2} - \frac{(1+q)}{M^{3/2}qu(2+k_1+k_2)} - \frac{1+k_2-k_1(1+q)}{(1+q)(2+k_1+k_2)}\,\delta\chi + \frac{\sqrt{\mathcal{C}}}{Mqu(2+k_1+k_2)}\right] \tag{30}$$

$$\mathcal{C} = 1+q\Big\{(q+1)^2(q+4)-(q+1)^2M^{3/2}u\left[\chi_{\rm cons}(k_1+k_2+2)+\delta\chi(k_1-k_2)\right]+qM^3u^2\left[\chi^2_{\rm cons}(k_1+k_2+2)+\delta\chi^2(1-k_1k_2)\right]\Big\}.$$

and

$$\frac{d\chi_{\rm cons}}{{\rm d}u} = -\frac{(1+q)^2\left\{2+q\left[4+2q+u(k_2-k_1)\delta\chi-u(2+k_1+k_2)\chi_{\rm cons}\right]\right\}}{u^2q(2+k_1+k_2)\left[(1+q)^2-2qu\chi_{\rm cons}\right]} \tag{31}$$

$$-\frac{(1+q)^2\left\{2\sqrt{(1+q)^4+q^2u^2[\delta\chi^2(1-k_1k_2)+\chi^2_{\rm cons}(2+k_1+k_2)]}-q(1+q)^2u[\delta\chi(k_1-k_2)+\chi_{\rm cons}(2+k_1+k_2)]\right\}}{u^2q(2+k_1+k_2)\left[(1+q)^2-2qu\chi_{\rm cons}\right]}.$$

By integrating Equations (29) and (31) we can fully describe the evolution of BNSs. Due to Equation (24) having no closed-form solution for its roots, this integration – which requires precession averaging at each step of u – is much slower and prone to numerical errors. Thus, our paper focuses on finding ways to make such calculations faster and robust for all BNS configurations.

F. Precessing BBH Evolutions

To help understand what evolving a binary system with the precession-averaged approach gives us, we present a couple outputs of the the `Precession` code. Figure 3 shows the evolution of the $\delta\chi$ bounds throughout a BBH inspiral from $r = 1000M$ to $r = 10M$. Figure 4 shows two gaussian-like distributions of κ values sampled from 500 binaries. In green are the κ values obtained from each binary configuration initialized at $r = 10M$, in red is the new distribution of κ values obtained from backward evolving each binary to $r = 1000M$.

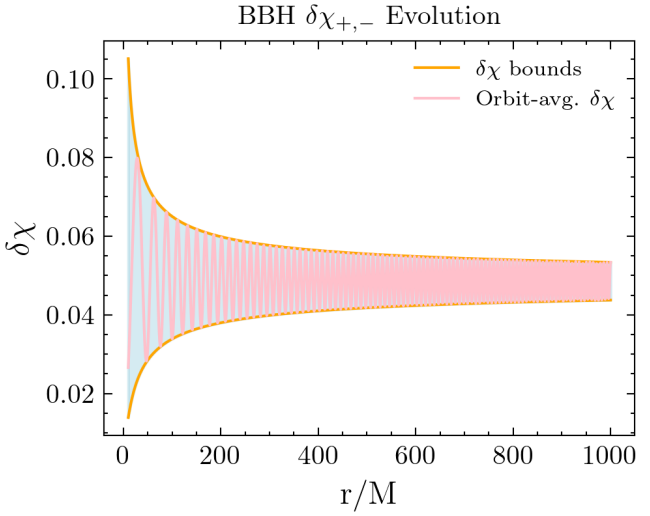


FIG. 3. $\delta\chi$ evolution of a BBH with initial conditions: $q = 0.88, \chi_1 = 0.26, \chi_2 = 0.11, \delta\chi = 0.05, \kappa = 0.06$, and $\chi_{\rm eff} = 0.11$. The orange lines show the precession bounds, $\delta\chi_{\{+,-\}}$, that precession averaging finds for us, in pink is the full evolution of $\delta\chi$ obtained from orbit averaging.

III. METHODS

A. Initial Root-Finding Optimizations

To find the roots of the right-hand side of Equation (24) we started by interpolating over $\delta\chi \in [-1, 1]$ with a cubic spline and finding the roots of the spline. In the BBH case, three roots could be found analytically, so we expect either to find three roots and keep the two that define the precession bounds – as in the BBH case – or we expect to get only two roots which define the precession bounds.

While this original spline approach was somewhat successful, it was not robust. Moreover, when using this method to evolve a binary, the time it would take to evolve was much longer than the BBH case – for BBHs evolutions take a fraction of a second, BNS evolutions with this method take a few to tens of seconds. This is quite problematic considering this greatly hinders the ability to do large population analyses of BNSs.

To remedy this we started investigating the behavior of each term in Equation (24). Although the roots of

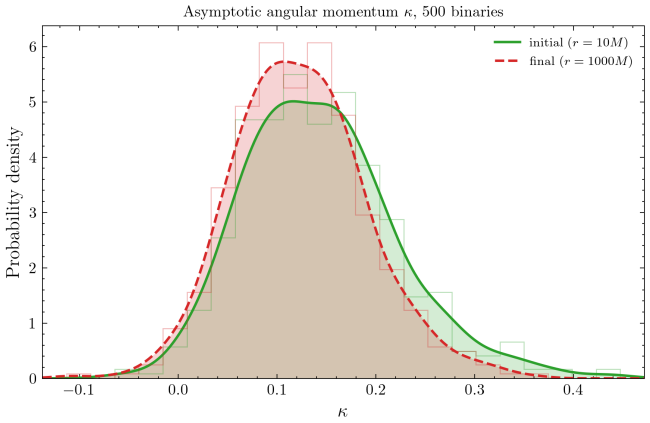


FIG. 4. Shown in green is a distribution of 500 BBH κ values at $r = 10M$. This was created by generating gaussian-like distributions of q, χ_1, χ_2, θ_1, θ_2, and $\Delta\Phi$, then drawing 500 samples from these distributions to generate 500 random binary configurations at $r = 10M$. In red we show what the final distribution of κ values are, obtained from backward evolving to $r = 1000M$. This process can be done for any parameter to study the evolution of that parameter for a distribution of binaries.

Equation (24) are not able to be found analytically, some of its terms have analytical solutions for their roots. The first three terms in Equation (24) all have analytical roots, and thus we looked to see if there was any common behavior in these functions that could be of use when looking for the roots of $\dot{\delta\chi}^2$.

In doing so, we noticed that the prefactor $\mathcal{A}^2$ never contributed physical roots, so we removed $\mathcal{A}^2$ from the interpolation. We also recognized that $\sin^2\Delta\Phi$ was always bounded within the region where $\sin^2\theta_1$ and $\sin^2\theta_2$ were both positive. Since $\dot{\delta\chi}^2$ is only defined when all three terms are defined, we only need to consider this smaller region. This led us to bound the spline of $\dot{\delta\chi}^2$ to the region where $\sin^2\theta_1$ and $\sin^2\theta_2$ are both positive, which is found using the analytical roots of those functions.

The bounded spline method was helpful because it sped up evolution times. It also made evolutions more robust across different cases due to a more refined grid on the physical region of $\dot{\delta\chi}^2$.

We also noticed that the roots of the spline of $\sin^2\Delta\Phi$ were the physical roots of $\dot{\delta\chi}^2$. This implies that the bounds of precession are determined by the points where $\Delta\Phi = 0$ or $\Delta\Phi = \pi$ – that is, when $\mathbf{S}_1$ and $\mathbf{S}_2$ are in plane with one another. A visualization of this overlap of roots, is shown in Figure 5.

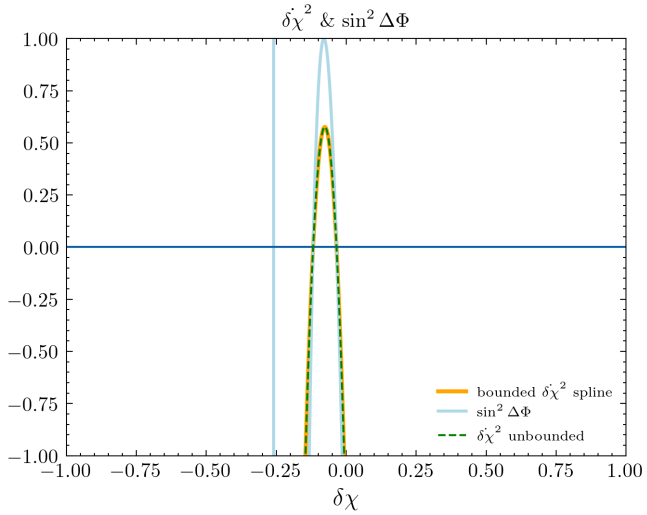


FIG. 5. Displayed above are plots of the unbounded and bounded splines of $\dot{\delta\chi}^2$ and $\sin^2\Delta\Phi$ over $\delta\chi \in [-1, 1]$ to visualize where the roots occur. This comes from a binary at $r = 1000M$ with $q = 0.78$, $\chi_1 = 0.74$, $\chi_2 = 0.57$, $k_1 = 2.22$, $k_2 = 3.97$, $\delta\chi = -0.09$, $\chi_{\rm cons} = 0.24$, and $\kappa = 0.12$. As can be seen, $\sin^2\Delta\Phi$'s roots are the same as $\dot{\delta\chi}^2$'s roots. Also, the bounded and unbounded spline agree. A pole at $\delta\chi \approx -0.25$ appears due to a root in $\sin^2\theta_1$ or $\sin^2\theta_2$ as $\sin^2\Delta\Phi$ is inversely proportional to both.

B. Finding a Polynomial Form of $\dot{\delta\chi}^2$

Rather than interpolating the long form of Equation (24), it is possible to rewrite it and obtain a polynomial form. First we introduce a few terms for future simplification, $\beta = 1 + q$, $\alpha = 2 + k_1 + k_2$, and $\eta = 2\sqrt{r}$. We also introduce $\gamma(\delta\chi)$,

$$\gamma(\delta\chi) = \big[(1 - k_1k_2)\delta\chi^2 + \eta(k_2 - k_1)\delta\chi + 4r - \eta\alpha\chi_{\rm cons} + \alpha\chi_{\rm cons}^2\big]^{1/2} \tag{32}$$

With this, we can make $\dot{\delta\chi}^2$ linear in $\gamma(\delta\chi)$,

$$\left(\frac{d\delta\chi}{dt}\right)^2 = A(\delta\chi) + B(\delta\chi)\gamma(\delta\chi)\,. \tag{33}$$

Now, if we consider the $(\delta\chi, \gamma)$ space we can look at the conic defined by γ^2. Call the radicand of γ, $G(\delta\chi)$. Then,

$$\gamma^2 - G(\delta\chi) = 0\,, \tag{34}$$

this conic in $(\delta\chi, \gamma)$ can be used like so: if we trace out the conic by taking the pencil of lines through a point on it, we obtain a free parameter s which can be related to $\delta\chi$. Then, rewriting Equation (33) with the relationship between $\delta\chi$ and s, we find a six-degree polynomial in s.

To go about this, we use the fact that $G(\delta\chi)$ is a quadratic and can be written as $G(\delta\chi) = c_2(\delta\chi - \delta\chi_G)(\delta\chi - \delta\chi'_G)$ where c_2 is the coefficient of $G(\delta\chi)$'s $\delta\chi^2$ term, and $\delta\chi_G$ and $\delta\chi'_G$ are the roots of $G(\delta\chi)$. Since the point $(\delta\chi_G, 0)$ lies on the conic we can parameterize it with the equation $\gamma = s(\delta\chi - \delta\chi_G)$ where s is a free parameter. Then,

$$\gamma^2 = c_2(\delta\chi - \delta\chi_G)(\delta\chi - \delta\chi'_G) = s^2(\delta\chi - \delta\chi_G)^2 \,. \quad (35)$$

Thus,

$$\delta\chi(s) = \frac{s^2\delta\chi_G - c_2\delta\chi'_G}{s^2 - c_2} \,, \quad (36)$$

and,

$$\gamma(s) = \frac{s(c_2)(\delta\chi_G - \delta\chi'_G)}{s^2 - c_2} \,. \quad (37)$$

Plugging these into Equation (33) one will find a six-degree polynomial in s. A full derivation of this process is presented in Ref [7]. The roots of this six-degree polynomial can be found much faster than by the interpolation method at the same accuracy, or sometimes better, and the s-roots can be converted to $\delta\chi$ roots with Equation (36) efficiently.

With this new method we find a much faster way to find the roots of $\dot{\delta\chi}^2$ and obtain the same roots in all cases. Note that this root-finding method assumes $k_i > 1$, so it is invalid for BBHs.

IV. RESULTS

A. Evolution optimization

At very large separations ($r > 10^5 M$), the root finder can fail. This is because at large separations the precession is not very pronounced, thus the $\delta\chi$ bounds are very close together and in some cases the polynomial root finder fails to differentiate between those nearby roots. Furthermore, as previously mentioned this approach is invalid for BBHs, and as we get to large enough separations the BNS system behaves like a BBH. Thus, the method may be breaking down due to the system converging to the BBH case.

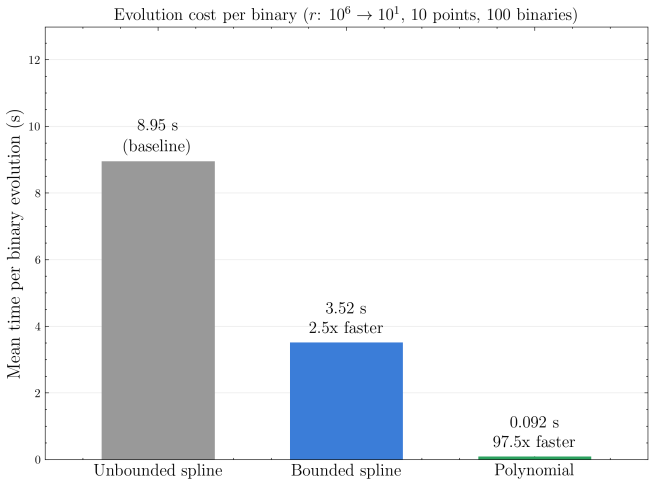


FIG. 6. Evolution speed comparison between the original spline approach, the bounded spline approach, and the polynomial form approach. 100 binaries were evolved from $r = 10^6 M$ to $r = 10M$ with 10 points in logspace on an 8-core M3 chip.

To fix this, we resort to the spline to handle an evolution where the polynomial approach fails at large r. Although this hybrid approach is not ideal, it works extremely well in most cases and still runs at bounded spline speeds for "failed" cases, a significant improvement from the start of this project. The speed up from this fix is shown in Figure 6. Compared to the original spline approach, we made evolutions 97.5× faster and more robust.

B. Comparing BNS and BBH $\delta\chi$ Evolutions

In Figure 7 we present some comparisons to a BBH evolution with the new BNS precession code. All three have the same binary setup, all that varies are the values of k_1 and k_2. As can be seen, the value of k – which is related to our object's tidal deformability – creates a significant impact on the precession cone. Further investigation of this impact and how it is manifested in waveforms may be an interesting avenue for future studies.

C. Bifurcations

With a much more robust and efficient way to evolve BNSs, we are able to investigate cases of BNS that bring about "bifurcations" in the spin evolution. A bifurcation

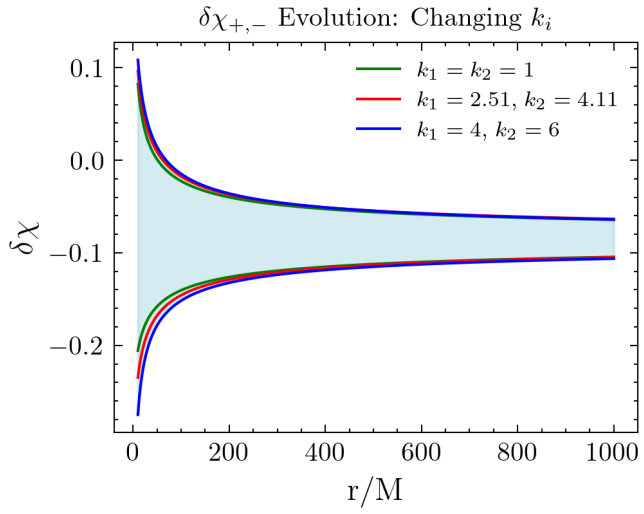


FIG. 7. Above is the evolution of the $\delta\chi$ bounds of a BBH in green, and two BNSs in red and blue. All three binaries were set up to evolve from $r = 1000M$ to $r = 10M$ with $q = 0.81$, $\chi_1 = 0.24$, $\chi_2 = 0.61$, $\delta\chi = -0.09$, and $\kappa = 0.001$. The BBH had a calculated $\chi_{\rm eff} = 0.01$. The BNSs had a calculated $\chi_{\rm cons} = 0.01$. The first BNS – in red – had k_i values determined by an APR EOS, this was calculated using the GW Python package `bilby.gw.eos`. The second BNS – in blue – had k_i values chosen manually for the sake of comparison. Notice that the precession bounds widen with increasing k_i for this binary configuration.

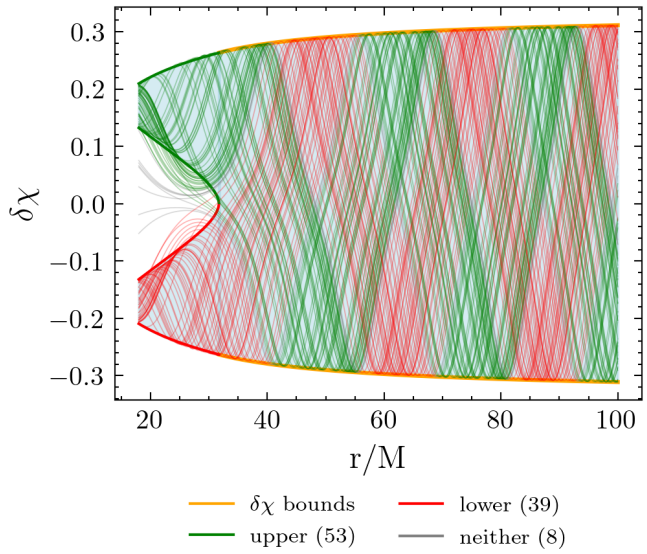


FIG. 8. A BNS with $q = \chi_1 = \chi_2 = 1$, $k_1 = k_2 = 10$, starting at $r = 10M$, $\kappa = 0.364$ and $\chi_{\rm cons} = 0.539$ shows a bifurcation in the precession cone at $r = 31.63M$. The faded green lines are orbit-averaged evolutions that ended up in the "upper" branch created after the bifurcation, similarly the faded red lines are orbit-averaged evolutions that end up in the "lower" branch. The gray lines are orbit-averaged evolutions that ended up in neither branch. The thick orange, green, and red bands are the bounds found from precession averaging.

is when a precession-averaged evolution hits a point where two precession cones are created, i.e. four roots of $\delta\chi$ are found. This creates an issue because the ordered pairs of roots create two possible branches for which the spins could evolve into. Moreover, when these bifurcations occur, the timescale hierarchy $t_{\rm pre} \ll t_{RR}$ is broken. We see a sharp spike in $t_{\rm pre}$ at the separation where the bifurcation occurs, and there $t_{\rm pre} > t_{\rm RR}$.

These bifurcations are not physical of course; for a given binary starting at some initial $\delta\chi$, orbit averaging will find a definite path for the binary's $\delta\chi$ to oscillate between. Thus, we hope to understand how to deal with these spin configurations as they are quite problematic. One of these bifurcations, accompanied by a range of orbit-averaged evolutions of the same binary starting at different initial $\delta\chi$'s, is shown in Figure 8.

We plan to continue investigating these bifurcations as they are unique to BNSs and have a large influence on the solution of the orbit-averaged evolutions. To do so we will scan the parameter space of initial BNS conditions to find when they occur, and hope that in doing so we can identify a trend that explains this behavior or shows us why the timescale hierarchy is breaking.

V. CONCLUSION

We developed an efficient framework to evolve precessing BNSs at speeds close to the `Precession` code which is specific to the simpler BBH case. Despite the unique cases of bifurcations, this method is robust for spinning ($\chi_{1,2} \in [0.1, 1)$) BNSs. We find a new configuration of spin precession evolutions, i.e. bifurcations, that result in the breaking of the assumed timescale hierarchy $t_{\rm pre} \ll t_{RR}$, these bifurcations require further study. In the future, with an understanding of these bifurcations, we expect that this work can be used to perform population studies of precessing BNS properties efficiently and grant us a way to study matter effects on BNS spin configurations.

VI. ACKNOWLEDGEMENTS

Thank you to my incredible mentors Giulia Fumagalli and Taylor Knapp. We thank Katerina Chatziioannou for overseeing this project and Davide Gerosa for developing the precession-averaged method to build off of. Lastly, thank you to LIGO SURF, Caltech Student Faculty Program, and the National Science Foundation for supporting our work over the summer.

[1] D. Gerosa, G. Fumagalli, M. Mould, G. Cavallotto, D. P. Monroy, D. Gangardt, and V. De Renzis, Efficient multi-timescale dynamics of precessing black-hole binaries, Phys. Rev. D **108**, 024042 (2023), arXiv:2304.04801 [gr-qc].

[2] T. A. Apostolatos, C. Cutler, G. J. Sussman, and K. S. Thorne, Spin-induced orbital precession and its modulation of the gravitational waveforms from merging binaries, Phys. Rev. D **49**, 6274 (1994).

[3] L. E. Kidder, Coalescing binary systems of compact objects to (post)$^{5/2}$-Newtonian order. V. Spin effects, Phys. Rev. D **52**, 821 (1995), arXiv:gr-qc/9506022 [gr-qc].

[4] É. Racine, Analysis of spin precession in binary black hole systems including quadrupole-monopole interaction, Phys. Rev. D **78**, 044021 (2008), arXiv:0803.1820 [gr-qc].

[5] D. Gerosa, M. Kesden, U. Sperhake, E. Berti, and R. O'Shaughnessy, Multi-timescale analysis of phase transitions in precessing black-hole binaries, Phys. Rev. D **92**, 064016 (2015), arXiv:1506.03492 [gr-qc].

[6] A. Klein, Efpe: Efficient fully precessing eccentric gravitational waveforms for binaries with long inspirals (2021), arXiv:2106.10291 [gr-qc].

[7] G. Fumagalli, T. Knapp, and Q. Kasdan-Grollo (2026), in preparation.